


Enhancement of excitonic and defect-related luminescence in neutron transmutation doped β -Ga₂O₃Curtis P. Irvine,¹ Attila Stopic^{1,2}, Mika T. Westerhausen,¹ Matthew R. Phillips,¹ and Cuong Ton-That^{1,*}¹*School of Mathematical and Physical Science, University of Technology Sydney, Ultimo, New South Wales 2007, Australia*²*ANSTO, Lucas Heights, New South Wales 2234, Australia* (Received 9 August 2022; revised 31 October 2022; accepted 16 November 2022; published 30 November 2022)

Neutron irradiation analysis, inductively coupled plasma mass spectrometry (ICPMS), and cathodoluminescence (CL) spectroscopy are used to investigate the influence of transmuted Ge incorporation on the luminescence properties of β -Ga₂O₃ single crystals. Calculations based on Ga₂O₃-neutron interaction reveal temporal variations of both Ge and Zn concentrations as a function of time during and after neutron irradiation. To produce a concentration of 5×10^{18} Ge donors/cm³ from the neutron transmutation of Ga, the β -Ga₂O₃ crystal was irradiated for 27 h, which was accompanied by the incorporation of 10^{16} Zn acceptors/cm³. These calculated dopant concentrations are confirmed by ICPMS. The β -Ga₂O₃ crystals exhibit a UV band at 3.40 eV due to self-trapped holes (STHs) and two blue donor-acceptor pair (DAP) peaks at 3.14 eV (BL1) and 2.92 eV (BL2). In addition to the neutron-induced incorporation of substitutional Ge donors and Zn acceptors on Ga sites, Ga vacancies (V_{Ga}) were created by high-energy neutrons in the flux, which strongly enhanced the BL1 peak. The V_{Ga} acceptors compensate the neutron-induced Ge donors, making the Ga₂O₃ crystal highly resistive. Concurrent temperature-resolved CL measurements of the β -Ga₂O₃ before and after neutron irradiation reveal a twofold increase in both the STH and BL1 peaks. This result suggests that STHs are preferentially localized at an O site adjacent to V_{Ga} , as theoretically predicted by Kananen *et al.* [*Appl. Phys. Lett.* **110**, 202104 (2017)]. Analysis of the Ga₂O₃ CL temperature dependence reveals that the UV and BL1 bands after the neutron irradiation exhibit an equivalent activation energy of 100 ± 10 meV due to the presence of a neutron-induced defect that acts as an efficient competitive nonradiative recombination channel. The results also provide evidence that the BL1 and BL2 bands arise from different DAP pairs.

DOI: [10.1103/PhysRevMaterials.6.114603](https://doi.org/10.1103/PhysRevMaterials.6.114603)

I. INTRODUCTION

Due to its ultrawide band gap (4.9 eV), large breakdown electric field, and radiation hardness, β -Ga₂O₃ is currently attracting great interest for use in electrical components for high-voltage and high-temperature operation, UV optoelectronics, and electronics in harsh surroundings, such as devices for extraterrestrial and nuclear reactor technologies [1]. However, only unipolar *n*-type Ga₂O₃ based devices have been fabricated so far because *p*-type doping at sufficiently high levels remains problematic. Conversely, controllable *n*-type doping of Ga₂O₃ has been achieved by the in-growth incorporation of Si, Sn, Ge, or H donors with activation energies (E_a) in the range of 16–60 meV [2–5]. These donors, as impurities, are considered to be likely candidates for the cause of the observed characteristic *n*-type conductivity in undoped Ga₂O₃ and can contribute to the low *p*-type doping efficiencies as acceptor compensators. There are two nonequivalent Ga atomic sites in β -Ga₂O₃ that are available for substitutional cation doping, Ga(I) and Ga(II) with tetrahedral and octahedral coordination geometry, respectively. Density functional theory (DFT) calculations show that Si and Ge donors preferentially occupy the Ga(I) site and act as shallow donors [6]. However, both shallow ($E_a = 34.9$ meV) and deep donor ($E_a = 120$ meV) states were found in Si-doped (010) β -Ga₂O₃ films

grown by metal organic chemical vapor deposition [7]. Neal *et al.* reported deep donors with ionization energies of 110 and 131 meV in commercial undoped (–201) β -Ga₂O₃ crystals from temperature dependent Hall effect and capacitance spectroscopy measurements [8,9]. Both these donor ionization energies were tentatively attributed to Si donors occupying the Ga(II) site, with the disparity in the donor energy being due to the use of different measurement techniques [8,10].

Photoluminescence (PL) and cathodoluminescence (CL) spectroscopy measurements of high-quality β -Ga₂O₃ single crystals and epilayers show a broad emission band that contains a UV band at 3.3 eV and blue luminescence (BL) bands at ~ 3.1 and ~ 2.8 eV; these bands have been attributed to self-trapped holes (STHs) and donor-acceptor pair transitions, respectively [11–14]. Cation vacancies are typically compensating acceptor defects in oxide semiconductors. Accordingly, Ga vacancies (V_{Ga}) are predicted to act as acceptors in β -Ga₂O₃ and are expected to play a critical role in the effort to achieve stable *p*-type doping and facilitate the fabrication of bipolar β -Ga₂O₃ devices. To date, however, the optical and electrical properties of vacancy defects in β -Ga₂O₃ bulk crystals have been the subject of much debate. Theoretical calculations by Ingebrigtsen *et al.* [15] reported that a Ga_{*i*}- V_{Ga} pair complex with three different structural configurations, labeled V_{Ga}^{ia} , V_{Ga}^{ib} , and V_{Ga}^{ic} , have low formation energies in *n*-type Ga₂O₃ and so are likely to be abundant deep acceptors. The split V_{Ga} modeling results have been supported by recent experiments [16,17]. Conversely, Ga_{*i*} shallow donors were

*cuong.ton-that@uts.edu.au

found to have a high formation energy, forming split energy levels at least 0.6 eV below the conduction band due to local atomic distortions [15].

Neutron transmutation doping is an established semiconductor doping technique that enables precise dopant concentrations with a highly uniform spatial distribution. For example, this technique has been used to homogeneously incorporate Ge in bulk GaN by the conversion of Ga into Ge after the capture of thermal neutrons. However, these Ge_{Ga} dopants in GaN could not be electrically activated even after annealing at 1000 °C, which was attributed to a structural displacement of Ge_{Ga} sites caused by the emission of nuclear particles [18,19]. Son *et al.* observed no neutral donor state in Si-doped Ga_2O_3 using electron spin resonance (ESR) spectroscopy and proposed that Si behaves like a DX-like donor state [20], which is a defect complex formed between the Si donor and a lattice defect labeled X. This DX-like complex was found to be highly stable and to be only partially activated after annealing at 1100 °C [20]. Studies of neutron and proton irradiation effects in Ga_2O_3 crystals and epilayers report the creation of several electrically active defect states across the entire band gap, although considerable controversy remains regarding the nature of defects induced by the irradiation [21–24]. Significantly, neutron irradiation has recently been used to homogeneously introduce V_{Ga} in $\beta\text{-Ga}_2\text{O}_3$ [21,25,26]. The photocurrent in Ga_2O_3 -based Schottky diodes was found to be strongly enhanced after neutron irradiation, which was explained by the introduction of V_{Ga} -related defects acting as hole traps [27]. Electron paramagnetic resonance (EPR) investigations of neutron-irradiated $\beta\text{-Ga}_2\text{O}_3$ reveal a hyperfine interaction of a trapped hole with two Ga neighboring atoms where the hole was found to be localized at a threefold-coordinated O site adjacent to V_{Ga} [26]. Studies of edge-defined film-fed (EFG) Ga_2O_3 crystals by deep-level transient spectroscopy and deep-level optical spectroscopy enabled the identification of a defect state associated with fast neutron irradiation at 1.29 eV below the conduction band edge [23]. Gao *et al.* [25,28] used CL to investigate Ga_2O_3 films grown by pulsed laser deposition (PLD) and low-pressure chemical vapor deposition (LPCVD). These studies reported broad emission bands centered at 3.0 and 2.5 eV, which increase in intensity after neutron irradiation, suggesting that V_{Ga} is involved in their transitions. Notably, the peak positions of these bands are different from the UV and BL bands observed in EFG-grown crystals. In this paper, we report a strong luminescence enhancement in $\beta\text{-Ga}_2\text{O}_3$ crystals following neutron irradiation. It is shown that Ga_2O_3 can be homogeneously doped with a precise Ge dopant concentration by thermal neutrons; however, the incorporated Ge donors are found to be strongly compensated by V_{Ga} acceptors produced by the presence of fast neutrons in the thermal neutron flux. Our results provide evidence for the involvement of V_{Ga} in both STH-related UV and blue defect emission peaks in neutron-irradiated $\beta\text{-Ga}_2\text{O}_3$.

II. EXPERIMENTAL DETAILS

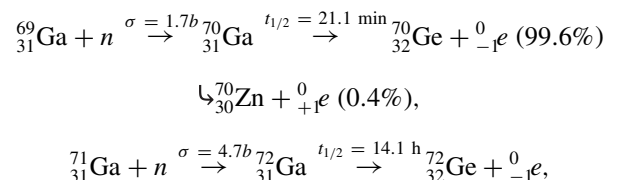
The samples used in this study are unintentionally doped (UID) Ga_2O_3 $10 \times 15 \times 0.68 \text{ mm}^3$ crystals grown by the EFG method (Tamura Corporation, Japan). The crystal possesses

the (−201) surface plane orientation and have been found to contain impurities of Si, Ir, and Al [29]. The crystal was placed inside an Al capsule and exposed to neutrons for 27 h in the irradiation facility in the OPAL Research Reactor at Australia’s Nuclear Science and Technology Organisation (ANSTO) [30]. The fluences of fast (energy > 0.5 MeV) and thermal neutrons (energy ~25 meV) were $\sim 1.03 \times 10^{18}$ and $1.25 \times 10^{19} \text{ cm}^{-2}$, respectively. Fast neutrons are used to induce vacancy formation, and thermal neutrons cause the transmutation of Ga into Ge. Notably, these neutron exposure conditions are similar to the irradiation conditions previously used to produce V_{Ga} [26]. The mean free path of fast neutrons in the energy range of 1 eV–20 MeV in Ga_2O_3 is >1 cm [31], which is significantly greater than the EFG crystal thickness of 0.68 mm. Before characterization studies were carried out, the irradiated crystal was left to decay for 11 months due to remnant radioactivity of unstable ^{192}Ir . Quantitative analysis of neutron-induced transmuted impurities was conducted using laser ablation inductively coupled plasma mass spectrometry (LAICPMS) using a New Wave Research NWR-193 excimer laser (Kennelec Scientific) coupled to an Agilent Technologies 7900 series ICPMS. Laser ablation was conducted by ablating 20 lines of 1 mm length using a 193 nm laser with a $150 \mu\text{m}$ spot scanning at $150 \mu\text{m s}^{-1}$ and pulsed at 40 Hz. Prior to data acquisition, the lines were preablated to remove any surface contamination. Standard reference materials NIST 610 and NIST 612 were used for the calibration of ICPMS. A NanoMagnetics Instruments ezHEMS system with a measurement limit of $10^9 \Omega \text{ cm}$ was used for electrical characterization. CL spectroscopy was performed using an FEI Quanta 200 scanning electron microscope (SEM) equipped with a custom CL spectroscopy setup, consisting of a parabolic mirror light collector and an Ocean Optics QE65000 spectrometer. Temperature dependent measurements were performed by mounting the Ga_2O_3 samples on an Oxford Instruments liquid nitrogen cold stage allowing low-temperature measurements from 80 to 300 K. All spectra were corrected for the total response of the CL measurement system. The electron beam current was measured using a Faraday cup in the sample stage.

III. RESULTS AND DISCUSSION

A. Neutron transmutation doping of Ga_2O_3

Neutron transmutation doping is a well-known method that produces homogeneous doping in bulk semiconductors with high precision [32]. Ga_2O_3 contains natural isotopes ^{69}Ga and ^{71}Ga with natural abundances of 60.2% and 39.8%, respectively. Unstable isotopes are formed from these Ga isotopes following exposure to neutron irradiation through the capture of thermal neutrons (n) and their subsequent decay to stable isotopes as follows [33]:



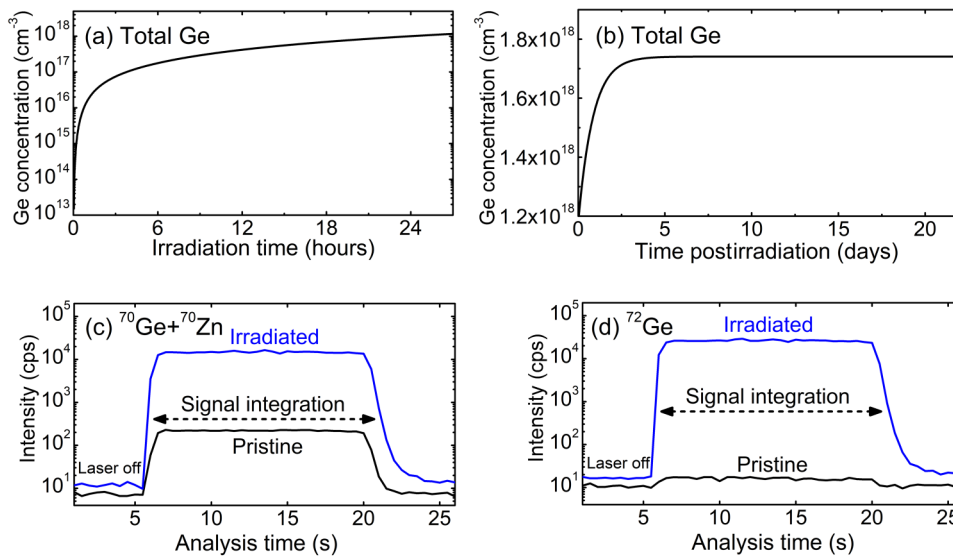


FIG. 1. (a) Calculated temporal transmuted Ge concentration in β -Ga₂O₃ with irradiation time. After 27 h of irradiation the crystal is doped with 1.2×10^{18} Ge atoms/cm³. (b) Calculated temporal transmuted Ge concentration as a function of time following the neutron irradiation. The Ge concentration increases within the first 5 days postirradiation and remains constant at 1.7×10^{18} atoms/cm³ afterward. (c,d) ICPMS signal traces for isotopes ⁷⁰Ge, ⁷⁰Zn, and ⁷²Ge from the laser ablation of the pristine and 27-h irradiated Ga₂O₃ crystals. Isotopes ⁷⁰Ge and ⁷⁰Zn cannot be distinguished due to spectral overlaps; however, the intensity increase following neutron irradiation is mostly (99.6%) due to the creation of the ⁷⁰Ge isotope. The ⁷²Ge signal intensity increases by three orders of magnitude upon the neutron irradiation.

where σ is the neutron capture cross section at 25.3 meV and $t_{1/2}$ is the lifetime calculated using the Evaluated Nuclear Data Format (ENDF) and NUDAT data libraries [34]. Unstable isotope ⁷⁰Ga can either beta decay to ⁷⁰Ge (99.6% probability) or electron capture to ⁷⁰Zn (0.4% probability) with $t_{1/2} = 21.1$ mins. ⁷²Ga beta decays with $t_{1/2} = 14.1$ h. The above parameters and an applied thermal neutron flux of 1.1×10^{14} cm⁻² s⁻¹ were used to calculate the concentration of transmutation Ge impurities according to standard equations [33]. The computed Ge concentration (the sum of ⁷⁰Ge and ⁷²Ge isotopes) produced as a function of time during and after neutron irradiation is shown in Figs. 1(a) and 1(b). The Ge concentration shows significant temporal dependence on the timescale of days, which should be taken into consideration for experimental study of neutron-irradiated Ga₂O₃ systems. The Ge concentration grows significantly within the first 5 days postirradiation due to the decay of the unstable ⁷⁰Ga and ⁷²Ga, which remains constant at 1.7×10^{18} atoms/cm³ afterward. The primary acceptor dopant formed in neutron-irradiated Ga₂O₃ is Zn; its concentration is found to increase substantially as unstable Ga and Cu isotopes decay and Zn is produced. The calculated Zn concentrations as a function of irradiation and postirradiation time are presented in the Supplemental Material, Fig. S1 [35]. The total Zn concentration postirradiation is 7.3×10^{15} atoms/cm³ for 27 h irradiation as depicted in Fig. S1(b) [35].

Chemical analysis was conducted using ICPMS to experimentally validate the transmutation calculation results. Raw ICPMS signal traces in counts per second (cps) for the isotopes ⁷⁰Ge and ⁷²Ge in the crystal before and after neutron irradiation are shown in Figs. 1(c) and 1(d). Each of the traces contains a stable plateau phase where the ablated material is constantly carried to the ICPMS; the signal from this plateau is used for quantitative analysis. Isotopes ⁷⁰Ge and ⁷⁰Zn can-

not be distinguished due to spectral overlaps; however, the intensity increase in Fig. 1(c) following neutron irradiation arises mostly (99.6%) from the formation of ⁷⁰Ge as shown in the above decay equations. The ⁷²Ge signal in the pristine Ga₂O₃ during laser ablation is only slightly higher than the laser-off background and its corresponding Ge concentration is about 0.13 ppm (7.0×10^{15} atoms/cm³). After the neutron irradiation, the ⁷²Ge intensity increases by three orders of magnitude and the measured Ge concentration in the irradiated crystal, averaged over 19 scans, is 97.5 ± 1.9 ppm ($5.2 \pm 0.1 \times 10^{18}$ atoms/cm³). Notably, this measured Ge concentration in the neutron-irradiated Ga₂O₃ is significantly higher than the calculated value, likely due to the matrix mismatch between the ICPMS standards and Ga₂O₃ crystal; however, the exact source of discrepancy is beyond the scope of this work. The flat plateau shape of the ICPMS profiles confirms that Ge is uniformly incorporated in the crystal. The crystal was also found to contain the expected Sn and Si impurities in a few parts per million ($\sim 10^{17}$ atoms/cm³) range [29], and the concentrations of these donors were unchanged following the neutron irradiation. From the Hall measurements, the carrier concentration of the pristine crystal was determined to be 2×10^{17} cm⁻³. Zn impurities were detectable by ICPMS in both the pristine and irradiated crystals. The Zn isotope traces, shown in Figs. S1(c) and S1(d) [35], all have signal intensities less than 5×10^2 cps. The ⁶⁶Zn and ⁶⁸Zn traces are considered to be equivalent for the pristine and irradiated crystals within the measurement uncertainty. The total measured Zn concentration is estimated to be $\sim 10^{16}$ cm⁻³ for both the crystals, consistent with the calculated transmuted Zn concentration. It is noted that the EFG Ga₂O₃ crystals used in this study contain a number of different metal impurities with concentrations up to 1 ppm, including Fe, Al, Cr, and Ir [29]. The amount of Zn measured by ICPMS in this work is about 0.3 ppm, which is not dissimilar to the concentrations of the reported metal im-

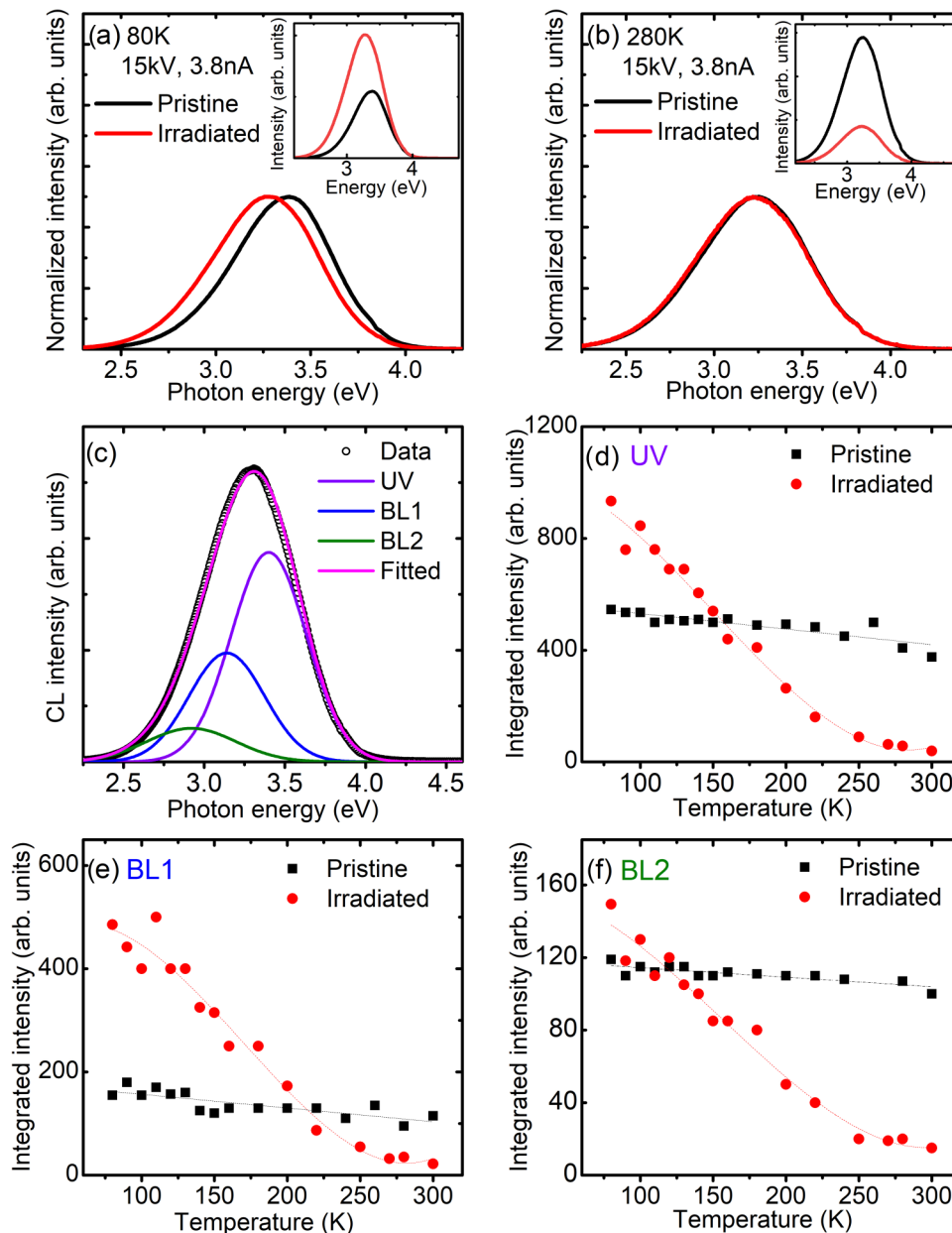


FIG. 2. (a,b) Normalized CL spectra of the pristine and neutron-irradiated β -Ga₂O₃ acquired under identical excitation conditions at (a) 80 K and (b) 280 K. The creation of V_{Ga} due to the neutron irradiation causes a redshift of 120 meV at 80 K, while the spectral shapes are identical at 280 K. The insets display the corresponding spectra before normalization, showing that the peak is enhanced at 80 K while it is quenched at 280 K. (c) A typical fitted spectrum of the irradiated Ga₂O₃ at 80 K using three Gaussian peaks labeled UV ($E = 3.40$ eV, $FWHM = 0.57 \pm 0.03$ eV), BL1 (3.14 eV, 0.55 ± 0.02 eV), and BL2 band (2.92 eV, 0.65 ± 0.02 eV). (d–f) Intensity versus temperature for the UV, BL1, and BL2 peaks in the pristine and irradiated β -Ga₂O₃ over the temperature range from 80 to 300 K. At 80 K, the intensity of the UV, BL1, and BL2 bands increases by a factor of 1.7, 3.2, and 1.3, respectively. With increasing temperature, the intensities of all three bands in the irradiated β -Ga₂O₃ are quenched rapidly because the thermal activation of neutron-induced defects mediates the UV, BL1, and BL2 emission intensities.

purities. The neutron-irradiated crystal is highly resistive, and its conductivity at room temperature could not be measured reliably due to the lower measurement limit of the electrometer, suggesting that Ge donors are strongly compensated by neutron-induced defects and Zn acceptors.

B. Neutron irradiation effects on luminescence properties

Normalized temperature-resolved CL spectra acquired from the β -Ga₂O₃ crystal under identical excitation

conditions (15 kV, 3.8 nA) before and after neutron irradiation at 80 and 280 K are shown in Figs. 2(a) and 2(b), respectively. As discussed below, the β -Ga₂O₃ CL spectra contain an intrinsic UV emission as well as two defect-related peaks in the blue spectral region. At 80 K, the CL emission peak of the entire CL spectrum located at 3.27 eV in the irradiated sample is redshifted by 120 meV compared with the emission maximum observed in the pristine crystal. This irradiation-induced redshift and associated CL emission broadening are caused by an

increase in the blue emission, compared with the intrinsic UV band, which is attributed to the creation of additional V_{Ga} defects. Conversely, Fig. 2(b) shows that the CL emission peak positions and shapes of the pristine and irradiated crystals at 280 K are identical due to complete thermal quenching of the STH UV emission. Previous studies of Zn-doped $\beta\text{-Ga}_2\text{O}_3$ show that a CL emission band at 2.7 eV is strongly influenced by the Zn incorporation [36]. However, no additional CL emission peaks appear over the entire temperature range up to 300 K after neutron irradiation due to incorporated Zn acceptors most likely due to its low 10^{16} cm^{-3} concentration. The insets of Figs. 2(a) and 2(b) also show the as-measured CL spectra at 80 and 280 K, revealing a luminescence enhancement at 80 K with the emission intensity increasing by a factor of more than 2, which is ascribed to additional V_{Ga} defects produced by the irradiation. This luminescence enhancement is remarkable as radiation-induced defect formation in semiconductors normally quenches the preexisting luminescence. As temperature increases, the CL emission of the irradiated crystal is quenched more rapidly than the pristine counterpart due to the thermal activation of nonradiative defects created by the neutron irradiation. Eventually at 280 K, the irradiated to pristine emission intensity ratio has decreased to 0.3 [see the inset in Fig. 2(b)] from its value of 2 at 80 K. Notably, previous investigations of neutron-irradiated $\beta\text{-Ga}_2\text{O}_3$ by other workers have confirmed the formation of deep-level defects after fast neutron irradiation [23]. Figures S2(a) and 2(b) [35] present plots of the CL peak position and overall full width at half maximum (FWHM) collected, respectively, from the pristine and irradiated $\beta\text{-Ga}_2\text{O}_3$ over the temperature range of 80–300 K, showing that the spectra are redshifted and broadened postirradiation across the entire temperature range. The FWHM of the emission from both the pristine and irradiated crystals steadily increases with rising temperature. The CL emission peak from the pristine crystal shifts rapidly towards lower energy with increasing temperature due to the thermal quenching of the STH UV emission. In contrast, the CL redshift in the irradiated crystal with temperature is minimal due to enhanced thermal stability of the STH UV peak caused by additional V_{Ga} defects.

In $\beta\text{-Ga}_2\text{O}_3$, holes can be trapped into strongly lattice coupled polaron states that can relax radiatively producing a broad Gaussian-like emission band [11,12]. Compared with the PL emission profile of the STH in $\beta\text{-Ga}_2\text{O}_3$ single crystals [peak energy $E = 3.37 \text{ eV}$, full wave at half maximum (FWHM) = 0.62 eV] [37], the measured CL spectra are significantly broader (see Fig. S2(b) [35]), indicating that additional defect-related emission is present in these spectra. In order to extract physically meaningful results from the CL spectra with highly overlapped peaks, spectral deconvolution was performed using conventional peak fitting techniques using the following procedure. First, the STH peak was fitted to the high-energy side of the spectrum using the peak position and FWHM reported for an isolated STH emission peak [37] [as shown in Fig. 2(c)] before deconvoluting the complete spectrum. Using this approach, the low-energy side of the emission spectrum was fitted with two broad defect-related Gaussian peaks labeled BL1 and BL2 using seed values from the literature (BL1: $E = 3.14 \text{ eV}$, FWHM = 0.60 eV; BL2: 2.92 eV, 0.65 eV) [11,38]. The BL1 peak energy matches

closely with the peak position found in the difference spectrum (Fig. S3 [35]), which is achieved by the subtraction of the pristine spectrum from the irradiated spectra after the pristine spectrum is scaled by 1.7 to account for the increase in the STH emission due to the neutron irradiation. This difference spectrum shows the neutron irradiation produces the most pronounced enhancement in the blue spectral region peaking at $\sim 3.14 \text{ eV}$. The two blue bands have been reported in the literature and ascribed to donor-acceptor pair (DAP) recombination channels involving deep acceptors such as isolated V_{Ga} and $(V_{\text{O}}-V_{\text{Ga}})$ defect pairs [12,13]. To improve the precision of the peak fitting method, the temperature dependence of the peak broadening of the defect-related BL peaks was included in the curve fitting process [12].

CL data were also acquired from different depths within the crystal by increasing the acceleration voltage. The beam current was adjusted so that the beam power ($17.3 \mu\text{W}$) was kept constant to produce the same e - h pair generation rate at each measurement voltage. The as-measured and normalized depth-resolved CL spectra for the pristine and irradiated crystals are shown in Figs. S4(a) and S4(b) [35]. The CL emission intensity is found to strengthen with increasing probe depth in both the pristine and irradiated crystals, suggesting that competitive nonradiative defects are present at the near surface region of the crystal most likely arising from residual surface polishing damage in the as-received sample. Notably, the normalized spectra reveal an identical peak shape and energy position with varying probe depth, confirming that both the UV and BL radiative centers are uniformly distributed throughout the crystal and that the neutron irradiation results in doping homogeneity.

Figures 2(d)–2(f) show plots of the CL intensity versus temperature between 80 and 300 K for the UV, BL1, and BL2 bands for the pristine and neutron-irradiated $\beta\text{-Ga}_2\text{O}_3$. The intensities of all three luminescence bands decrease with increasing temperature as competitive nonradiative transitions are thermally activated. However, a considerably faster decay is observed in the irradiated $\beta\text{-Ga}_2\text{O}_3$, suggesting that a highly efficient competitive nonradiative defect is created by the neutron irradiation that mediates the radiative recombination kinetics of the UV and BL bands in neutron-irradiated $\beta\text{-Ga}_2\text{O}_3$. The enhancement of the blue bands in the irradiated $\beta\text{-Ga}_2\text{O}_3$ can be explained by the creation of defects as a result of exposure to fast neutrons [23,26], which leads to additional BL1 and BL2 recombination centers in the irradiated crystal. The luminescence behaviors of the BL1 and BL2 bands upon the neutron irradiation and their temperature profiles are different [see Figs. 2(e) and 2(f)], confirming they originate from different electronic transitions. Remarkably, the UV STH band is also enhanced at temperatures below 150 K upon the neutron irradiation, which suggests that the presence of V_{Ga} can strongly influence the formation and stability of STHs in $\beta\text{-Ga}_2\text{O}_3$. Previous EPR studies revealed that ionized V_{Ga} exhibits a hyperfine structure consistent with the localization of one or two holes on adjacent O atoms [26]. Consequently, the neutron-induced creation of V_{Ga} defects can conceivably provide a mechanism to increase the hole concentration and so account for the increased UV STH emission post-neutron irradiation. Also, the increase of V_{Ga} -related acceptors will compensate the irradiation-induced n -type Ge doping, which

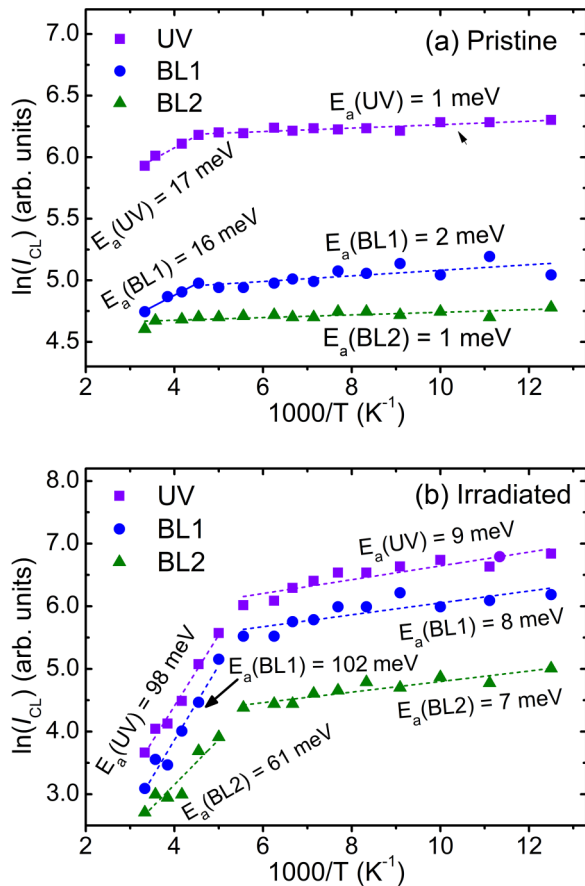


FIG. 3. Arrhenius plots of $\ln(I_{CL})$ versus $1000/T$ and linear analysis of the UV, BL1, and BL2 integrated intensities for the (a) pristine and (b) neutron-irradiated β -Ga₂O₃. Straight lines are fitted separately to lower and upper temperature ranges above and below 200 K, yielding the activation energies E_a as indicated. The activation energies of the UV and BL1 bands are equivalent at 100 ± 10 meV for the irradiated β -Ga₂O₃, respectively, indicating the emission intensity bands are mediated by a new neutron-induced defect. In the low-temperature range (< 200 K), all the emission bands possess much smaller activity energies, ~ 1 meV for the pristine crystal and ~ 8 meV for the irradiated crystal, which is most likely due to a phonon-assisted quenching process.

explains the high electrical resistivity of the crystal after the neutron exposure.

Arrhenius analysis of the UV, BL1, and BL2 bands is performed to determine the activation energy of their electronic transitions as illustrated in Fig. 3. The existence of two distinct linear temperature ranges extending from 80 to 200 K and 200 to 300 K for both the pristine and neutron-irradiated β -Ga₂O₃ reveals the presence of two separate activation processes. Straight lines are fitted to each of the linear regions over the lower and upper temperature ranges, yielding activation energies summarized in Table I. Below 200 K, the UV, BL1, and BL2 bands possess small activation energies at $E_a \approx 1$ and 8 meV for the pristine and irradiated Ga₂O₃, respectively. These weak temperature dependences of three luminescence bands are likely due to thermal quenching associated with a phonon-assisted excitation of localized defect states, similar

TABLE I. Activation energies obtained from the Arrhenius analysis of the integrated peak intensity data for UV, BL1, and BL2 for temperatures above and below 200 K.

Peak	Activation energy (meV)	
	Pristine crystal	
	Below 200 K	Above 200 K
UV 3.40 eV	1.2 ± 0.2	17 ± 2
BL1 3.14 eV	2.0 ± 0.6	16 ± 1
BL2 2.92 eV	0.9 ± 0.2	–
Neutron-irradiated crystal		
UV 3.40 eV	9.5 ± 1.5	98 ± 6
BL1 3.14 eV	8.2 ± 1.8	102 ± 10
BL2 2.92 eV	7.2 ± 1.6	62 ± 11

to the mechanism observed in other oxides at low temperatures [39]. The activation energy of 17 meV above 200 K in the pristine crystal is within the binding energy range of 17–50 meV reported for shallow Sn and Si donors [40], which are the main impurities in EFG β -Ga₂O₃ crystals. Post-neutron irradiation, the activation energy is observed to increase to ~ 100 meV for the UV and BL1 bands and ~ 60 meV for the BL2 emission at temperatures beyond 200 K. The irradiation-induced increase of the CL emission is attributed to changes in the local deformation environment where holes are stabilized in the vicinity of an ionized V_{Ga} defect [26]. Notably, the 100 meV activation energy in the neutron-irradiated β -Ga₂O₃ is comparable with the previously reported ionization energies of 110 meV for an unintentional donor in the EFG β -Ga₂O₃ crystal [8] and at 120 meV in Si-doped β -Ga₂O₃ [7]. The chemical nature of this deep donor has not been conclusively identified in the literature; interstitials, antisites, and Si or Ge occupying the octahedral Ga(II) site have been suggested to be responsible for this donor state [8,10]. The measured 100 meV activation energy is significantly smaller than the thermal activation energy of Zn_{Ga} acceptors at both Ga(I) and Ga(II) sites, which is at least 0.65 eV [41]. This activation energy is also much smaller than the reported ionization energies of both V_O and V_{Ga} [42]; thus these vacancy defects can be ruled out as its origin. Computational studies predict that the Si occupation is thermodynamically favorable on the Ga(I) over the Ga(II) site [6]. In contrast to equilibrium crystal growth techniques, Ge doping by neutron-induced Ga transmutation occurs under nonequilibrium conditions and Ge donors are incorporated on both Ga(I) and Ga(II) sites equally. Therefore, Ge(II) donors are abundant in neutron-induced Ge-doped β -Ga₂O₃ and their concentration in the irradiated crystal should be $\sim 2.6 \times 10^{18}$ atoms/cm³ from the ICPMS results. By analogy to Si doping, Ge(II) donors would have similar ionization energy to the Si on a Ga(II) site, so accordingly the 100 meV activation energy measured after the neutron irradiation could be related to Ge donors on the Ga(II) site. It is plausible that the incorporated Ge in the irradiated crystal behaves like a localized DX-like donor state formed by the recoil of β particles in the decay of the Ga isotopes (see the decay equations in Sec. III A). DX-like donor states have previously been identified in GaN after neutron

irradiation [18,43]; however, there are conflicting ESR [20] and electrical transport measurement [40] results that support and refute, respectively, the presence of DX-like donor states in β -Ga₂O₃.

The luminescence intensities of the CL bands in the β -Ga₂O₃ crystals were measured as a function of excitation density (beam current, I_B) before and after neutron irradiation. The UV and BL emissions were found to exhibit remarkably similar excitation-power dependencies as I_B was increased over three orders of magnitude from 0.1 to 10 nA while the beam energy was kept constant at $E_B = 15$ keV. Increasing I_B in this range did not introduce any noticeable changes in peak shape or energy position (see Figs. S5(a) and S5(b) [35]). The power density analysis for the pristine and irradiated β -Ga₂O₃ crystals is illustrated in a log-log plot (Figs. S4(c) and S4(d) [35]) using a simple power-law model $I_{CL} \propto I_B^k$, where I_{CL} is the integrated peak intensity, k is the power-law exponent, and I_B is the e -beam current. Power-law fits reveal identical k values within the measurement error for the three bands with $k_{\text{pristine}} = 0.90 \pm 0.03$ and $k_{\text{irradiated}} = 0.99 \pm 0.02$ for the pristine and irradiated crystals, respectively. Power-law exponents around $k \cong 1$ are characteristic of excitonic and band-to-band transitions, which exhibit fast recombination rates. Conversely, recombination involving deep levels, such as free-to-bound transitions, typically display much smaller k values of ~ 0.5 due to their slow relaxation kinetics, arising from strong lattice coupling [44]. Accordingly, the measured $k \cong 1$ value for the BL1 and BL2 peaks is consistent with their assignment to DAP rather than free-to-bound transitions and provides an insight into the nature of the BL emission bands in Ga₂O₃.

A DAP emission band comprises multiple highly overlapped peaks, each corresponding to each of the discrete lattice distances r between the donor and the acceptor involved in the radiative transition. The DAP emission energy is given by [45,46],

$$hv(\text{DAP}) = E_g - (E_A + E_D) + \frac{e^2}{4\pi\epsilon\bar{r}}, \quad (1)$$

where E_A and E_D are the donor and acceptor binding energies, respectively. The last term accounts for the Coulombic interaction between the ionized donor and ionized acceptor with r being their separation distance. Assuming a random distribution of donor-acceptor pairs, the average distance \bar{r} can be estimated as $\bar{r} = \sqrt[3]{\frac{3}{4\pi N_{D/A}}}$, where $N_{D/A}$ is the higher N_D or N_A density [46,47]. Furthermore, the transition probability $P(r)$ of the DAP pairs decreases exponentially with increasing r as

$$P(r) = P(r_{\min}) \exp\left(-\frac{2\bar{r}}{r_B}\right), \quad (2)$$

where r_B is the larger of the donor or acceptor Bohr radius [48]. Consequently, a DAP band typically blueshifts and changes shape with increasing I_B since more distant pairs saturate more quickly than closer pairs and so no longer contribute the total DAP emission peak. The lack of a DAP blueshift with increasing excitation (I_B) can occur when predominantly close pairs are involved in the DAP transition. This can occur when either (i) the DAP involves a deep donor and a deep acceptor

with highly localized wave functions or (ii) the donor and/or acceptor doping level is high, reducing \bar{r} and increasing the transition probability, as described in Eq. (2). In this case, the latter reason applies since high concentrations of Ge, Sn, and Si donors above 10^{17} cm⁻³ exist in the crystal, as shown by ICPMS. This DAP assignment is also consistent with the increase in the power-law exponent towards $k \approx 1$ postirradiation (see Fig. S5 [35]) as more V_{Ga} acceptors are produced by fast neutrons.

An estimation of the donor concentration, N_D , in the Ge-doped Ga₂O₃ can be made using the energy position of the most enhanced BL1 peak at 3.14 eV due to the creation of neutron-induced V_{Ga} . Furthermore, for the production of V_{Ga} and Ga_i defect pairs via a knock-on effect by fast neutrons, all three V_{Ga}^i split structural configurations are possible, with their acceptor energy E_A in the range 1.62–1.69 eV [15]. Although the specific donor defect responsible for the BL1 DAP transition in the irradiated β -Ga₂O₃ cannot be unequivocally identified, the logical candidate is transmuted Ge that acts as a shallow donor in the irradiated crystal. Using $E_D \approx 30$ meV for the donor energy of Si and Ge [40,49], and $E_A \leq 1.69$ eV for the V_{Ga} split configurations, Eq. (1) yields $\bar{r} \gtrsim 14$ nm, which corresponds to $N_D \leq 8 \times 10^{16}$ cm⁻³. While the donor concentration of the neutron-irradiated crystal could not be measured using electrical measurements due to its high resistivity, this N_D value is two orders of magnitude lower than the ICPMS measured total Ge concentration of 5.2×10^{18} atoms/cm³, suggesting transmuted Ge donors are heavily compensated by irradiation-induced acceptors V_{Ga} and Zn_{Ga} . Notably, previous studies showed Si-doped Ga₂O₃ epitaxial films with similar Si concentrations (up to 4×10^{18} cm⁻³) were still nonconducting electrically [50]. The second blue band BL₂ at ~ 2.9 eV has been previously attributed to DAP involving V_{Ga} -related acceptors in single crystals [51] or Zn_{Ga} acceptors in Zn-doped Ga₂O₃ [36]. However, our experimental results do not support the involvement of V_{Ga} as the BL₂ intensity only exhibits a modest intensity increase post-neutron irradiation at temperatures below 120 K even though the irradiation produces a substantial increase in the V_{Ga} concentration. The electrical conductivity of β -Ga₂O₃ was previously found to decrease while the photocurrent in β -Ga₂O₃ Schottky diodes increased after exposure to fast neutrons; these findings were ascribed to the creation of predominantly V_{Ga} defects by fast neutrons [27,52]. It is likely that the BL₂ DAP involves either V_{O} donors or (V_{O} - V_{Ga}) acceptor complexes because the concentration of these defects would remain unchanged after the neutron irradiation. The higher BL₂ recombination rate with its k value rising from 0.87 to 0.99 postirradiation (see Fig. S5 [35]), together with the Ge doping results by ICPMS, suggests that the BL₂ DAP could arise from Si/Ge donors and (V_{O} - V_{Ga}) acceptor complexes, as defined by Eq. (2). However, further work is required to confirm these defect assignments. Thermal annealing at temperatures up to 700 °C in argon was attempted to remove the neutron-irradiation-induced vacancies in the crystal but was found to be ineffective as no changes in the luminescent and electrical properties were detected after the annealing treatment. This result suggests that V_{Ga} and other defects produced by neutron irradiation exhibit a high thermal stability.

IV. CONCLUSIONS

Neutron irradiation and chemical analyses in this work show that thermal neutron irradiation can be used to incorporate Ge donors into β -Ga₂O₃ by the transmutation decay of lattice Ga cations that have captured thermal neutrons. This finding potentially opens the door for uniform Ge doping, where the Ge concentration can be precisely controlled by varying the irradiation period and postirradiation time. However, neutron irradiation also creates V_{Ga} and Zn_{Ga} acceptors, reducing the carrier density. Furthermore, the intensity of the STH UV emission at 80 K is enhanced by approximately twofold post-neutron irradiation; this enhancement indicates that neutron-induced V_{Ga} centers can stabilize holes in β -Ga₂O₃ and supports the theoretically predicted model of holes being trapped at O ions adjacent to a Ga vacancy. The most pronounced CL enhancement due to the neutron irradiation is the blue DAP band at 3.14 eV, where the donor is a shallow Ge donor state, and the acceptor is a $\text{Ga}_i\text{-}V_{\text{Ga}}$ pair complex. Significantly, this blue band and the STH UV emission

in the irradiated β -Ga₂O₃ exhibit identical temperature dependencies with a similar activation energy of ~ 100 meV, indicating that their recombination is mediated by an efficient nonradiative defect, which is likely a DX-like Ge center in which Ge is situated at the octahedral Ga(II) site. This nonradiative defect acts as a competitive recombination center that controls the recombination kinetics in neutron Ge-doped Ga₂O₃. Our findings illustrate the importance of using an array of complementary characterization techniques to fully understand the neutron transmutation doping process in Ga₂O₃.

ACKNOWLEDGMENTS

This work was supported under the Australian Research Council (ARC) Discovery Project funding scheme (Project No. DP210101146). The authors acknowledge the support of ANSTO in providing access to the neutron irradiation facility used in this work via Proposal No. AP12165 and thank Herbert Yuan for technical support with SEM analysis.

-
- [1] S. J. Pearton, J. Yang, P. H. Cary IV, F. Ren, J. Kim, M. J. Tadjer, and M. A. Mastro, *Appl. Phys. Rev.* **5**, 011301 (2018).
- [2] T. T. Huynh, E. Chikoidze, C. P. Irvine, M. Zakria, Y. Dumont, F. H. Teherani, E. V. Sandana, P. Bove, D. J. Rogers, M. R. Phillips, and C. Ton-That, *Phys. Rev. Mater.* **4**, 085201 (2020).
- [3] M. Higashiwaki, K. Sasaki, T. Kamimura, M. H. Wong, D. Krishnamurthy, A. Kuramata, T. Masui, and S. Yamakoshi, *Appl. Phys. Lett.* **103**, 123511 (2013).
- [4] K. Irmischer, Z. Galazka, M. Pietsch, R. Uecker, and R. Fornari, *J. Appl. Phys.* **110**, 063720 (2011).
- [5] N. Moser, J. McCandless, A. Crespo, K. Leedy, A. Green, A. Neal, S. Mou, E. Ahmadi, J. Speck, K. Chabak, N. Peixoto, and G. Jessen, *IEEE Electron Device Lett.* **38**, 775 (2017).
- [6] J. B. Varley, J. R. Weber, A. Janotti, and C. G. Van de Walle, *Appl. Phys. Lett.* **97**, 142106 (2010).
- [7] Z. Feng, A. Anhar Uddin Bhuiyan, M. R. Karim, and H. Zhao, *Appl. Phys. Lett.* **114**, 250601 (2019).
- [8] A. T. Neal, S. Mou, R. Lopez, J. V. Li, D. B. Thomson, K. D. Chabak, and G. H. Jessen, *Sci. Rep.* **7**, 13218 (2017).
- [9] S.-S. Huang, R. Lopez, S. Paul, A. T. Neal, S. Mou, M.-P. Houng, and J. V. Li, *Jpn. J. Appl. Phys.* **57**, 091101 (2018).
- [10] K. Iwaya, R. Shimizu, H. Aida, T. Hashizume, and T. Hitosugi, *Appl. Phys. Lett.* **98**, 142116 (2011).
- [11] Y. S. Wang, P. T. Dickens, J. B. Varley, X. J. Ni, E. Lotubai, S. Sprawls, F. Liu, V. Lordi, S. Krishnamoorthy, S. Blair, K. G. Lynn, M. Scarpulla, and B. Sensale-Rodriguez, *Sci. Rep.* **8**, 18075 (2018).
- [12] T. T. Huynh, L. L. C. Lem, A. Kuramata, M. R. Phillips, and C. Ton-That, *Phys. Rev. Mater.* **2**, 105203 (2018).
- [13] T. Onuma, S. Fujioka, T. Yamaguchi, M. Higashiwaki, K. Sasaki, T. Masui, and T. Honda, *Appl. Phys. Lett.* **103**, 041910 (2013).
- [14] L. Binet and D. Gourier, *J. Phys. Chem. Solids* **59**, 1241 (1998).
- [15] M. E. Ingebrigtsen, A. Y. Kuznetsov, B. G. Svensson, G. Alfieri, A. Mihaila, U. Badstubner, A. Perron, L. Vines, and J. B. Varley, *APL Mater.* **7**, 022510 (2019).
- [16] A. Karjalainen, V. Prozheeva, K. Simula, I. Makkonen, V. Callewaert, J. B. Varley, and F. Tuomisto, *Phys. Rev. B* **102**, 195207 (2020).
- [17] J. M. Johnson, Z. Chen, J. B. Varley, C. M. Jackson, E. Farzana, Z. Zhang, A. R. Arehart, H. L. Huang, A. Genc, S. A. Ringel, C. G. Van de Walle, D. A. Muller, and J. Hwang, *Phys. Rev. X* **9**, 041027 (2019).
- [18] K. Kuriyama, T. Tokumasu, J. Takahashi, H. Kondo, and M. Okada, *Appl. Phys. Lett.* **80**, 3328 (2002).
- [19] A. Polyakov, N. Smirnov, A. Govorkov, A. Markov, S. Pearton, N. Kolin, D. Merkurisov, V. Boiko, C.-R. Lee, and I.-H. Lee, *J. Vac. Sci. Technol., B* **25**, 436 (2007).
- [20] N. Son, K. Goto, K. Nomura, Q. Thieu, R. Togashi, H. Murakami, Y. Kumagai, A. Kuramata, M. Higashiwaki, and A. Koukitu, *J. Appl. Phys.* **120**, 235703 (2016).
- [21] S. Bhandari, C. Nardone, and M. Zvanut, *J. Appl. Phys.* **132**, 025701 (2022).
- [22] M. E. Ingebrigtsen, J. B. Varley, A. Y. Kuznetsov, B. G. Svensson, G. Alfieri, A. Mihaila, U. Badstubner, and L. Vines, *Appl. Phys. Lett.* **112**, 042104 (2018).
- [23] E. Farzana, M. F. Chaiken, T. E. Blue, A. R. Arehart, and S. A. Ringel, *APL Mater.* **7**, 022502 (2019).
- [24] M. Chang, D. Guo, X. Zhong, F. Zhang, and J. Wang, *J. Appl. Phys.* **132**, 123105 (2022).
- [25] H. Gao, S. Muralidharan, N. Pronin, M. R. Karim, S. M. White, T. Asel, G. Foster, S. Krishnamoorthy, S. Rajan, L. R. Cao, M. Higashiwaki, H. Wenckstern, M. Grundmann, H. Zhao, D. C. Look, and L. J. Brillson, *Appl. Phys. Lett.* **112**, 242102 (2018).
- [26] B. E. Kananen, L. E. Halliburton, K. T. Stevens, G. K. Foundos, and N. C. Giles, *Appl. Phys. Lett.* **110**, 202104 (2017).
- [27] E. Yakimov, A. Polyakov, I. Shchemerov, N. Smirnov, A. Vasilev, P. Vergeles, E. Yakimov, A. Chernykh, A. Shikoh, and F. Ren, *APL Mater.* **8**, 111105 (2020).
- [28] H. T. Gao, S. Muralidharan, M. R. Karim, S. M. White, L. R. Cao, K. Leedy, H. P. Zhao, D. C. Look, and L. J. Brillson, *J. Phys. D: Appl. Phys.* **53**, 465102 (2020).

- [29] A. Kuramata, K. Koshi, S. Watanabe, Y. Yamaoka, T. Masui, and S. Yamakoshi, *Jpn. J. Appl. Phys.* **55**, 1202A2 (2016).
- [30] S. J. Kennedy, *Phys. B (Amsterdam)* **385**, 949 (2006).
- [31] H. Meriaty, Characterisation of the Neutron Field at the ANSTO Instrument Calibration Facility, Australian Nuclear Science & Technology Organisation, ANSTO, Australia (2009).
- [32] C. H. Seager and T. G. Castner, *J. Appl. Phys.* **49**, 3879 (1978).
- [33] M. A. Vesaghi, *Phys. Rev. B* **25**, 5436 (1982).
- [34] <https://www.nndc.bnl.gov>.
- [35] See Supplemental Material at <http://link.aps.org/supplemental/10.1103/PhysRevMaterials.6.114603> for additional characterization results.
- [36] I. López, M. Alonso-Orts, E. Nogales, and B. Méndez, *Phys. Status Solidi A* **215**, 1800217 (2018).
- [37] S. Yamaoka, Y. Mikuni, and M. Nakayama, *J. Phys.: Conf. Ser.* **1220**, 012030 (2019).
- [38] K. Shimamura, E. G. Villora, T. Ujiie, and K. Aoki, *Appl. Phys. Lett.* **92**, 201914 (2008).
- [39] Z. Lin, W. Chen, R. Zhan, Y. Chen, Z. Zhang, X. Song, J. She, S. Deng, N. Xu, and J. Chen, *AIP Adv.* **5**, 107229 (2015).
- [40] A. T. Neal, S. Mou, S. Rafique, H. P. Zhao, E. Ahmadi, J. S. Speck, K. T. Stevens, J. D. Blevins, D. B. Thomson, N. Moser, K. D. Chabak, and G. H. Jessen, *Appl. Phys. Lett.* **113**, 062101 (2018).
- [41] T. D. Gustafson, J. Jesenovec, C. A. Lenyk, N. C. Giles, J. S. McCloy, M. McCluskey, and L. E. Halliburton, *J. Appl. Phys.* **129**, 155701 (2021).
- [42] T. Lovejoy, R. Chen, X. Zheng, E. Villora, K. Shimamura, H. Yoshikawa, Y. Yamashita, S. Ueda, K. Kobayashi, and S. Dunham, *Appl. Phys. Lett.* **100**, 181602 (2012).
- [43] P. Boguslawski and J. Bernholc, *Phys. Rev. B* **56**, 9496 (1997).
- [44] C. Ton-That, L. Weston, and M. R. Phillips, *Phys. Rev. B* **86**, 115205 (2012).
- [45] D. G. Thomas, J. J. Hopfield, and W. M. Augustyniak, *Phys. Rev.* **140**, A202 (1965).
- [46] K. Thonke, T. Gruber, N. Teofilov, R. Schonfelder, A. Waag, and R. Sauer, *Phys. B (Amsterdam)* **308**, 945 (2001).
- [47] F. Williams, *Phys. Status Solidi B* **25**, 493 (1968).
- [48] A. Vink, *J. Lumin.* **9**, 159 (1974).
- [49] T. Jiao, Z. Li, W. Chen, X. Dong, Z. Li, Z. Diao, Y. Zhang, and B. Zhang, *Coatings* **11**, 589 (2021).
- [50] D. Gogova, G. Wagner, M. Baldini, M. Schmidbauer, K. Irmscher, R. Schewski, Z. Galazka, M. Albrecht, and R. Fornari, *J. Cryst. Growth* **401**, 665 (2014).
- [51] T. Onuma, Y. Nakata, K. Sasaki, T. Masui, T. Yamaguchi, T. Honda, A. Kuramata, S. Yamakoshi, and M. Higashiwaki, *J. Appl. Phys.* **124**, 075103 (2018).
- [52] L. Cojocar, *Radiat. Eff.* **21**, 157 (1974).